科学通报 2017 年 第 62 卷 第 20 期: 2262 ~ 2278
专题: 二维材料与器件(Ⅰ) 评 述
《中国科学》杂志社
SCIENCE CHINA PRESS

二维材料异质结的可控制备及应用

肖遥[1], 江贝[2], 杨柯娜[2], 张涛[2], 付磊[1,2*]

1. 武汉大学高等研究院, 武汉 430072;
2. 武汉大学化学与分子科学学院, 武汉 430072
* 联系人, E-mail: leifu@whu.edu.cn

2016-12-05 收稿, 2017-01-11 修回, 2017-01-18 接受, 2017-04-25 网络版发表
国家自然科学基金(21473124, 21673161)和中德科学中心基金(GZ871)资助

摘要 二维材料异质结是由石墨烯、六方氮化硼、过渡金属二硫族化合物、黑磷等二维材料通过面内拼接或层间堆叠形成的, 并由此可分为二维材料面内异质结和垂直异质结. 二维材料面内异质结可以实现区域内载流子的特殊传输行为; 而垂直异质结中的层间量子耦合效应能够导致新颖的物理特性, 通过调节异质结构界面可调制器件的电学及光学性能. 目前, 随着电子器件、光电器件等对集成性、功能性的要求不断提高, 二维材料异质结越来越多地受到研究者的关注, 实现二维材料异质结结构(包括界面)的有效调控是构筑高性能、高集成器件的前提. 本文主要对比各类二维材料异质结的制备方法, 介绍主流的几类二维材料异质结基电子器件和光电器件的结构、工作原理和性能, 展望有前景的新型制备方法, 并指出二维材料异质结在实际应用中面临的挑战.

关键词 二维材料异质结, 剥离法, 化学气相沉积法, 电子器件, 光电器件

从2004年石墨烯的成功获得开始[1], 具有层状结构的二维材料(如石墨烯、六方氮化硼(h-BN)、过渡金属二硫族化合物(TMDCs)、黑磷(BP)等)逐渐进入人们的视野, 其较于块体材料往往显示出独特的性质[2~4]. 然而, 单一的二维材料在应用时往往存在一定的局限, 例如, 绝缘层与石墨烯或TMDCs之间的电荷陷阱会严重影响优异电学性质的展现[5], h-BN带隙过宽(约5.97 eV[6])难以单独应用于器件中, 裸露的BP在空气中易被氧化导致其性能衰减. 为了深入研究材料本征性质并扩展其应用领域, 研究者将目光放在了二维材料异质结上. 二维材料异质结是由二维材料通过面内拼接或层间堆叠形成, 主要包括石墨烯/h-BN异质结、TMDCs/h-BN异质结、TMDCs/石墨烯异质结、TMDCs/TMDCs异质结等[7]. 垂直异质结中, 石墨烯/h-BN垂直异质结主要是利用h-BN减少绝缘层与石墨烯之间的电荷陷阱, 提升石墨烯中载流子的迁移率[8]; TMDCs/石墨烯垂直异质结主要结合TMDCs的光响应性和石墨烯的高导电性, 应用于高性能光响应器件; TMDCs/TMDCs垂直异质结主要是结合两种材料不同的能带结构, 控制载流子传输行为、实现存储或高性能的光响应. 面内异质结要求材料晶格失配度低, 一般用于研究材料界面处的载流子传输行为. 本文简介了二维材料的分类和性质以及二维材料异质结的制备方法(图1), 并对各类方法进行了评估. 同时, 针对目前制备方法中存在的界面污染等问题, 介绍了新兴的液态金属化学气相沉积法(LMCVD), 揭示了该方法对于推动二维材料异质结可控制备的重要意义. 此外, 本文综述了基于二维材料异质结的电子器件和光电器件的结构和原理. 最后, 本文对如何实现二维材料异质结的可控制

引用格式: 肖遥, 江贝, 杨柯娜, 等. 二维材料异质结的可控制备及应用. 科学通报, 2017, 62: 2262–2278
Xiao Y, Jiang B, Yang K N, et al. Controllable synthesis of two dimensional heterostructures and their application (in Chinese). Chin Sci Bull, 2017, 62: 2262–2278, doi: 10.1360/N972016-01348

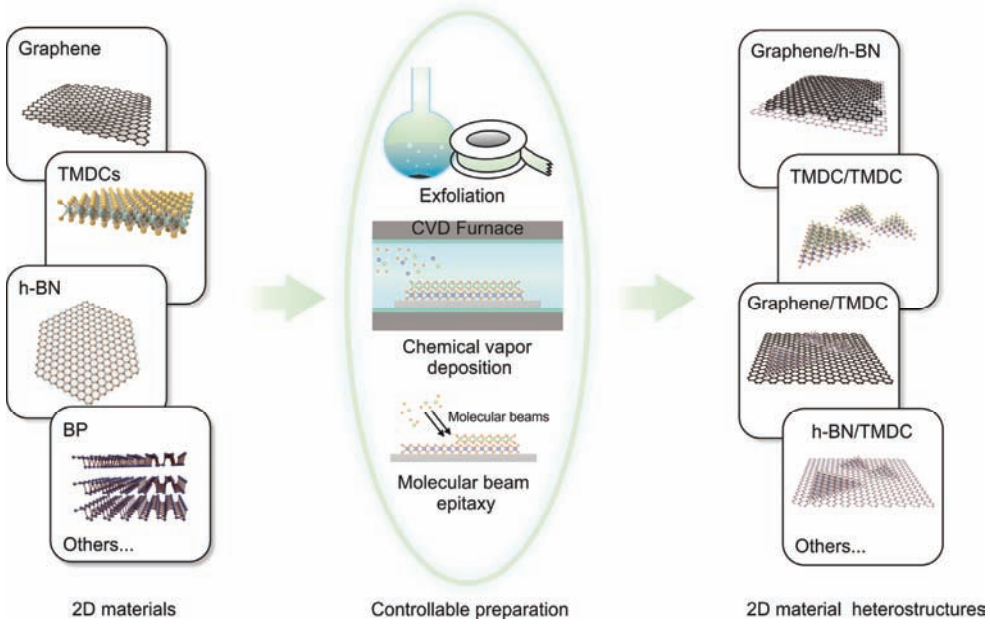

图 1 (网络版彩色)二维材料(2D materials)异质结的可控制备

Figure 1 (Color online) Controllable preparation of 2D material heterostructures

备以及其广阔的应用前景进行了展望.

1 二维材料的分类

1.1 石墨烯

石墨烯是由sp^2型杂化的碳原子构成的六方蜂巢状结构. 它具有众多优异性质, 如比表面积大(2630 $m^2\ g^{-1}$)[9]、电子迁移率高(200000 $cm^2\ V^{-1}\ s^{-1}$)[2]、杨氏模量高(~1.0 TPa^{-1})[10]、热导率高(~5000 $W\ m^{-1}\ K^{-1}$)[11]、透光率高(~97.7%)[12]. 石墨烯的制备方法包括机械剥离法和化学剥离法[13~15]、氧化还原法[16,17]、SiC外延法[18,19]和CVD法[20~22]等. 目前, 石墨烯已广泛应用于电子器件、能源存储与转换、传感等领域[23~25].

1.2 TMDCs

TMDCs的化学通式是MX_2, 其中M代表IVB族(Ti, Zr, Hf等)、VB族(V, Nb, Ta等)、VIB族(Mo, W等)的过渡金属元素, X代表硫族元素(S, Se或Te)[26,27], M和X原子构成X–M–X的层状结构. TMDCs依据性质的不同可分为绝缘体(HfS_2)、半导体(MoS_2, WS_2)、半金属(WTe_2, $TiSe_2$)和超导体($NbSe_2$, TaS_2). TMDCs的合成方法主要包括CVD法和剥离法[28,29]. 目前, TMDCs可以被应用于光电器件、电子器件、催化、能源存储等领域[30,31].

1.3 h-BN

h-BN是由B原子和N原子交替排列形成的层状二维原子晶体, 具有优良的绝缘性和化学稳定性. h-BN与石墨烯晶格失配度仅1.7%, 适于构筑面内异质结[6,32]. 此外, 通过与石墨烯形成异质结, 具有平滑、惰性表面的h-BN可以消除传统SiO_2绝缘层的电荷陷阱[33,34], 有助于提高石墨烯的载流子迁移率. 目前, h-BN主要的合成方法有机械剥离法、CVD法和共偏析法[35~37]. 相较于机械剥离法, CVD法和共偏析法更能满足大尺寸器件的需求[6]. 目前, h-BN可以作为电子器件中的电介质材料[33,38]、抗氧化涂料[39~41]和紫外光学材料[34,42,43]等.

1.4 其他二维材料

除了石墨烯、TMDCs和h-BN之外, 许多新型二维材料也被陆续制得. 理论预测表明, 硅烯具有与石墨烯类似的零带隙, 锗烯是金属型材料[44]. 硅烯、锗烯和锡烯一般通过在金属或石墨表面外延生长制备得到[45~49], 目前基于硅烯和锗烯的场效应晶体管(FETs)已有报道[50,51], 理论上还可应用于锂离子电池[52]. 由单元素组成的二维材料还有BP和硼烯. BP是一种各向异性的p型半导体材料, 根据层数不同具有0.3~2.0 eV的带隙[53,54], 弥补了TMDCs等半导体材料带隙范围的空白, 与此同时, 它还有较高的载流子

迁移率(~10^4 cm^2 V^{-1} s^{-1})[55]. 制备BP的方法一般是剥离法, 并用氧化物等材料进行保护[54,56]. BP目前已经在FETs、光电检测器等领域有了广泛的应用, 并表现出优良的性能. 而硼烯是由B原子组成的薄膜, 具有高硬度、高稳定性和优良的热电性质. 硼烯可以通过CVD法在Cu表面制备获得, 其具有2.25 eV的带隙, 是一种非常有应用前景的材料[57]. 除此之外, 还有过渡金属碳化物(TMCs), 如具有优异的超导性质的Mo_2C等[58,59]; 第IIIA族的硫族化合物, 如GaSe[60]; 过渡金属氮化物(TMNs), 如MoN_2[61]. 其中部分材料还处于理论预测阶段[61], 有待进一步研究.

2 二维材料异质结的可控制备

二维材料异质结分为垂直异质结[7]和面内异质结[62], 分别通过层间堆叠和面内拼接形成. 二维材料异质结的制备方法主要包括剥离法、CVD法和分子束外延(MBE)法. 剥离法主要是采用聚合物辅助将剥离得到的二维材料转移堆叠到一起形成异质结[63]. 这种方法可以获得高质量、单层的二维材料, 但其层数和面积均难以控制, 并且定点转移难度高, 在转移过程中还会引入缺陷和杂质. MBE法则克服了剥离法中转移的困难, 利用分子束直接在基底上外延制备二维材料异质结, 可以实现大面积和高质量的制备[64], 而此法对于基底平整性要求严苛, 且分子束获得较为困难. 相比剥离法和MBE法, CVD法对基底选择限制较少、方法简单、成本低, 且得到的材料质量高[65]. 二维材料异质结可以通过剥离法和CVD法结合制得[66], 也可以直接全由CVD法制得. CVD法直接制备二维材料异质结是将前驱体一同放入石英管中, 通过控制不同前驱体的进样时间、反应温度和时间、载气流量等, 最终可以在基底上获得二维材料的垂直异质结或面内异质结. CVD法制备异质结有望实现大批量生产, 但难以避免的杂质及表面缺陷令人困扰. 近期, 本课题组[67,68]发展了一系列基于液态金属的CVD方法用以获得高质量的二维材料异质结: 基于Ni–Ga合金的抗硫化特性及高催化活性, 采用CVD法获得了高质量的MoS_2/h-BN异质结; 利用TMDCs的伴生生长行为, 实现了100%堆垛的TMDCs垂直异质结的可控制备. 基于液态金属的异质结制备方法有效解决了传统CVD法存在的杂质残留和剥离法的界面污染问题, 获得了高质量、界面洁净的二维材料异质结.

2.1 石墨烯/h-BN异质结的可控制备

h-BN具有高化学惰性、高温稳定性、高机械强度和低介电常数等特点, 且表面原子级平滑、无悬挂键和带电杂质, 若与石墨烯形成异质结, 有望显著提高石墨烯基器件的性能.

目前垂直异质结的构筑方式主要是层层转移, 但此法难以实现大面积制备且成本很高, 转移过程中界面的污染和材料破损往往不可避免. 因此, 通过CVD法直接制备异质结将是一个更好的选择. Liu课题组[69]使用Co基底首先生长了h-BN, 然后再使用等离子辅助的方法生长石墨烯, 同时获得石墨烯和h-BN的面内异质结和垂直异质结. 北京大学刘忠范课题组[70]提出共偏析法直接一步法构筑石墨烯/h-BN异质结, 如图2(a)所示, 在C掺杂的Ni膜和Ni膜之间预植B和N源, 并对其进行真空退火, 从而形成垂直堆垛的石墨烯/h-BN异质结. 这种方法能够有效避免接触界面的污染. Johnson课题组[62]在Cu上生长了石墨烯/h-BN面内异质结, 证明了h-BN是倾向于沿着石墨烯边缘生长的(图2(b)), 只有小部分会在Cu上形成孤立的三角形片层, 由此可以得出对于h-BN的生长, 石墨烯的边缘比裸露的Cu箔活性更高. Suenaga课题组[71]制备了按照不同方式进行拼接的石墨烯和h-BN面内异质结(图2(c)). Song课题组[72]则提出了一种新颖的h-BN/石墨烯/h-BN异质结的构筑形式, 并研究了不同基底对h-BN生长机制的影响. 这种生长方式保护了中间层石墨烯, 避免了杂质污染, 有利于构筑高性能器件.

2.2 TMDCs/h-BN异质结的可控制备

使用h-BN作为TMDCs的基底, 得到TMDCs/h-BN异质结, 可以有效避免基底效应, 使TMDCs的光电性能得到明显改善. 通常可以通过将MoS_2等TMDCs转移至h-BN上来构筑异质结, 但这类方法难以实现大面积制备. 直接生长TMDCs/h-BN异质结是努力的方向, 改进h-BN, TMDCs生长方法和设计独特的生长基底均可实现高质量TMDCs/h-BN异质结的制备.

Warner课题组[73]采用CVD法生长MoS_2和h-BN, 如图3(a)所示. 通过拉曼和光致发光(PL)光谱分析, 研究发现h-BN上直接生长的MoS_2相较于生长在SiO_2/Si上而后转移的MoS_2, 具有更小的晶格应变和更低的掺杂能, 同时这种直接生长的异质结拥有更强的界面相互作用和更少的界面污染. Zettl课题组[66]

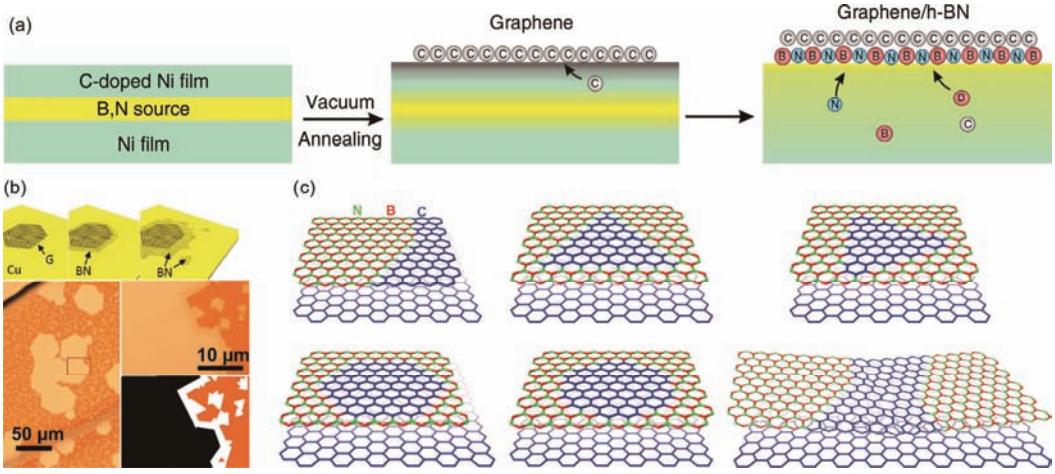

图 2 (网络版彩色)石墨烯/h-BN异质结的制备. (a) 共偏析法生长石墨烯/h-BN异质结示意图[70]; (b) 铜基底上h-BN沿石墨烯的边缘外延生长[62]; (c) 石墨烯和h-BN的各种拼接方式示意图[71]

Figure 2 (Color online) Preparation of graphene/h-BN heterostructures. (a) Schematic illustrating the growth of graphene/h-BN heterostructures via co-segregation method[70]; (b) the epitaxial growth of h-BN along the edge of graphene on Cu foil[62]; (c) schematic illustrating the different stitching ways between graphene and h-BN[71]

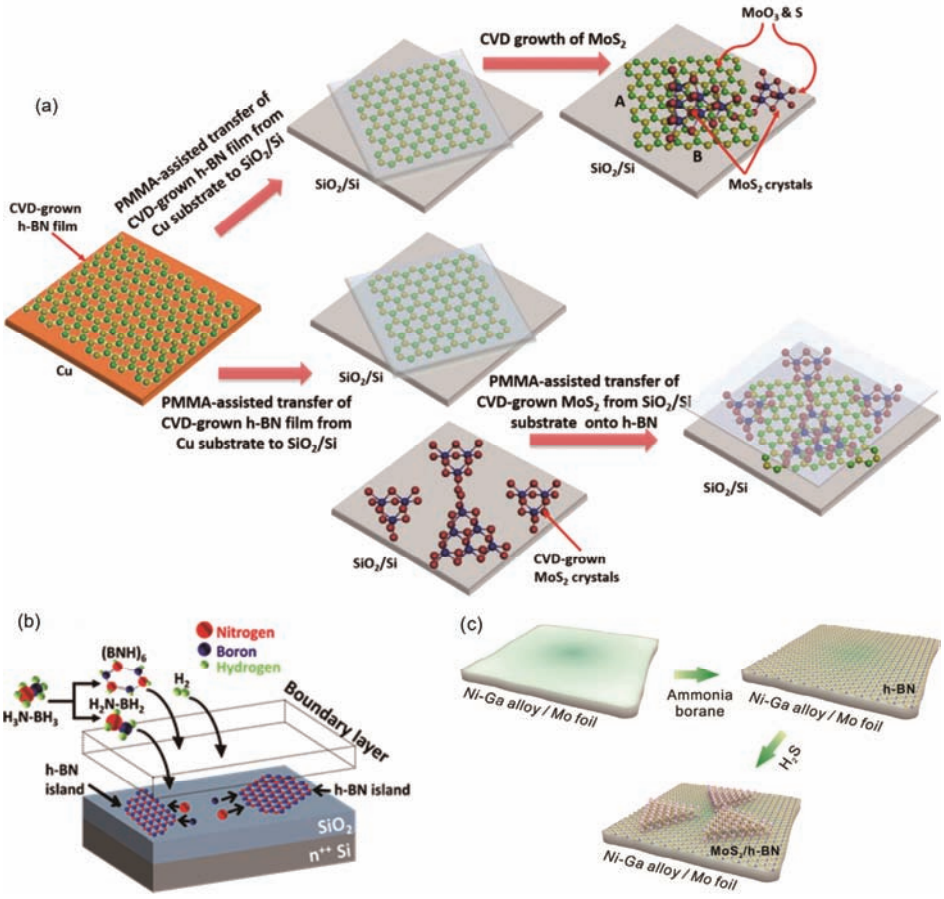

图 3 (网络版彩色)TMDCs/h-BN异质结的制备. (a) 两种常见的构筑MoS_2/h-BN异质结的方法示意图[73]; (b) SiO_2/Si上CVD生长h-BN的机理示意图[74]; (c) 抗硫化合金上生长MoS_2/h-BN异质结的示意图[67]

Figure 3 (Color online) Preparation of TMDCs/h-BN heterostructures. (a) Schematic illustrating the common methods for the preparation of MoS_2/h-BN heterostructures[73]; (b) schematic illustrating the growth mechanism of h-BN on SiO_2/Si[74]; (c) schematic illustrating the fabrication of MoS_2/h-BN heterostructures *via* sulfide-resistant alloy[67]

也在h-BN上合成了单层或多层MoS_2, 此法生长的单层MoS_2能保持自身的原有性质, 对于构筑基于MoS_2的高质量器件非常有利. Berry课题组[74]提出一种氧辅助合成大面积均匀超薄h-BN的方法, 如图3(b)所示, 并基于这种h-BN膜生长TMDCs/h-BN异质结, 该方法可以有效地降低界面粗糙度并减少杂质的引入. 而对于TMDCs生长方法的改进, Granozzi课题组[75]通过改变温度调控WS_2的构型, 获得无定型WS_2与2H-WS_2的混合物, 进而组成WS_2/h-BN异质结. 这种方法可以扩展至其他TMDCs/h-BN异质结的制备. 国家纳米科学中心谢黎明课题组[76]通过调控前驱体$ZrCl_4$的蒸发温度, 在h-BN上生长出了层数可控的ZrS_2. 最近, 本课题组[67]使用Ni基抗硫化合金实现了MoS_2/h-BN垂直异质结的直接CVD生长. 如图3(c)所示, 首先在Ni–Ga基底上催化生长h-BN, 然后在H_2S的作用下直接形成MoS_2/h-BN异质结. 这种方法能够获得TMDCs和h-BN平滑干净的界面和强的层间相互作用, 并且可以适用于其他TMDCs/h-BN异质结的生长.

2.3 TMDCs/石墨烯异质结的可控制备

TMDCs/石墨烯异质结结合了石墨烯高的载流子迁移率和TMDCs的高开关比、高光响应的优点, 在电子、光电器件领域有着广阔的应用前景. 构筑高效TMDCs/石墨烯异质结基器件的关键在于如何避免界面污染以及增强界面相互作用力.

Kong课题组[77]在石墨烯上低温(400 ℃)生长了MoS_2, 得到了MoS_2/石墨烯异质结, 利用原子力显微镜(AFM)观察到MoS_2从独立的单晶到生长成膜的过程, 通过扫描透射电子显微镜(STEM)发现, MoS_2的衍射取向趋向于与石墨烯的衍射保持一致, 并且石墨烯上外延的MoS_2能够作为催化和电子氧化还原中心. Ulstrup课题组[78]在超高真空下在石墨烯上制备了MoS_2, 并研究了其界面的电子状态, 证明MoS_2能够基本不受下层石墨烯的影响保持自身的带隙结构. Hersam课题组[79]则在石墨烯上采用CVD生长了旋转对称且层数可控的MoS_2, 而且通过拉曼光谱和X射线衍射(XRD)证明MoS_2几乎不受应力作用, 同时也证明外延石墨烯是范德华外延生长其他二维材料的良好基底. Robinson课题组[80]通过同样的方法得到了MoS_2/石墨烯、WSe_2/石墨烯和h-BN/石墨烯异质结, 并通过拉曼光谱等表征证实准自支撑的外延石墨烯(QFEG)中残余应变和褶皱对于上层的成核是非常有利的, 有助于形成高质量的异质结膜, 且基于MoS_2/QFEG异质结的光传感器的响应度有所提升. Tsuji课题组[81]则设计了一种MoS_2/石墨烯异质结, 通过外延生长MoS_2单晶来判断多晶石墨烯的晶界. 北京大学张艳锋课题组[82]采用CVD法在Au上先后生长了全覆盖的单层石墨烯和单层MoS_2纳米片, 构筑了MoS_2/石墨烯异质结. 石墨烯的存在可以有效地减弱MoS_2和Au间作用力, 保留了MoS_2的固有性质. 石墨烯和Au的弱相互作用有利于制备的异质结向任意基底转移, 拓展了器件的应用范围.

2.4 TMDCs/TMDCs异质结可控制备

半导体单层TMDCs已被广泛用于构筑p-n结和其他光学器件, 由这些二维材料通过堆叠或拼接形成的各类异质结往往表现出性能的提升, 而如何制备具有洁净平滑表面和取向精确控制的异质结仍是个不小的挑战.

香港中文大学徐建斌课题组[65]使用常压CVD (APCVD)生长了MoS_2/WS_2面内异质结, 采用两种水溶性盐分别作为Mo源和W源进行两步生长(图4(a)). 由于原料廉价易得, 可扩展至多种二维材料异质结生长, 可实现大面积生长, 该方法利于其在光电器件领域的应用. Li课题组[83]则通过外延生长得到接触界面原子级平滑的MoS_2/WSe_2面内异质结, 并对其应力作用进行了研究, 发现随着MoS_2的外延生长, 其应力作用逐渐增强, 而远离内层WSe_2的区域则逐渐不受应力作用, 如图4(b)中PL光谱所示. 图4(c)所示为MoS_2的A_{1g}和E_{2g}振动频率图, 基于这种应力作用的异质结构筑的器件有望在光电领域获得广泛应用. 相对于上述的单一堆垛形式的异质结, Ajayan课题组[84]通过控制温度实现了MoS_2与WS_2的不同堆垛, 包括垂直异质结与面内异质结, 图4(d)和(g)分别为其垂直异质结和面内异质结的示意图, 图4(e)和(h)为对应的光学显微图, 从扫描电子显微镜(SEM)图(图4(f)和(i))可以看出其表面无明显污染物. 类似的还有Johns课题组[85]利用氢气调控MoS_2与WS_2的堆垛方式, 引入H_2会使MoS_2边缘更光滑, 有助于形成面内异质结; 而不通H_2时, 已生长的MoS_2边缘有一些小颗粒, 利于WS_2在MoS_2表面成核从而形成垂直异质结. Ajayan课题组[86]也获得了一种同时存在面内和垂直异质结的结构, 两步生长过程中, WSe_2先沿着$MoSe_2$边缘生

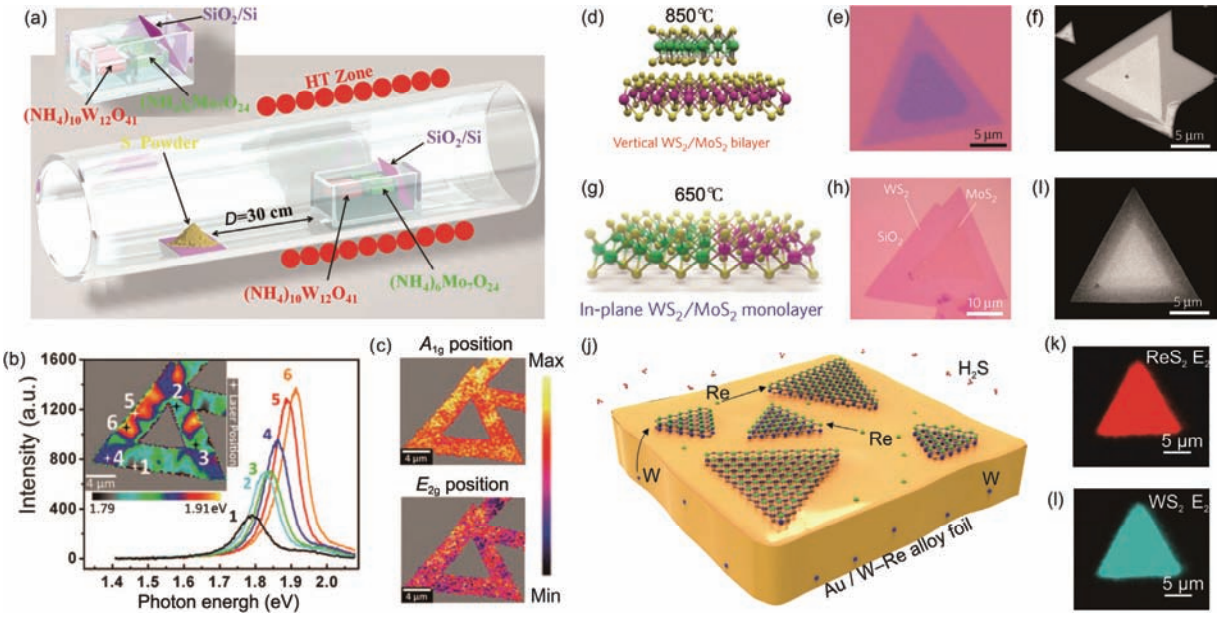

图 4 (网络版彩色)TMDCs/TMDCs异质结的制备及表征. (a) APCVD法制备WS_2/MoS_2异质结的示意图[65]; (b) WSe_2/MoS_2异质结中MoS_2的PL光谱; (c) MoS_2的A_{1g}和E_{2g}峰的拉曼光谱面扫图[83]; (d) 850℃下生长得到的WS_2/MoS_2垂直异质结的结构示意图; (e), (f) 图(d)对应的垂直异质结的光学显微镜图和SEM图; (g) 650℃下生长得到的WS_2/MoS_2面内异质结的结构示意图; (h), (i) 图(g)对应的面内异质结的光学显微镜图和SEM图[84]; (j) 液态金属CVD伴生生长WS_2/ReS_2垂直异质结的方法示意图; (k), (l) WS_2/ReS_2异质结中ReS_2和WS_2的E_{2g}振动的拉曼光谱面扫图[68]

Figure 4 (Color online) Synthesis and characterizations of TMDCs/TMDCs heterostructures. (a) Schematic illustrating the preparation of WS_2/MoS_2 heterostructures by APCVD[65]; (b) the PL properties of MoS_2 in WSe_2/MoS_2 heterostructures; (c) Raman mapping of peak position corresponding to the A_{1g} and E_{2g} mode of MoS_2[83]; (d) schematic illustrating the structure of vertical WS_2/MoS_2 heterostructures grown at 850°C; (e), (f) corresponding optical microscope (OM) and SEM images of the vertical WS_2/MoS_2 heterostructures illustrated in (d); (g) schematic illustrating of the structure of lateral WS_2/MoS_2 heterostructures grown at 650°C; (h), (i) corresponding OM and SEM of lateral WS_2/MoS_2 heterostructures illustrated in (g)[84]; (j) schematic illustrating the twinned growth of WS_2/ReS_2 heterostructure via a liquid Au CVD strategy; (k), (l) Raman mappings of peak intensity for corresponding to the E_{2g} mode of ReS_2 and WS_2 respectively[68]

长后又在其表面垂直生长, 形成了同时具有面内拼接和垂直堆垛的异质结, 这种两步法生长可以有效地避免交叉污染, 并且这种异质结具有良好的光响应.

值得一提的是, 本课题组[68]首次发现了TMDCs独特的伴生生长行为, 并利用其实现了100%堆垛的垂直异质结的可控制备(图4(j)). 以ReS_2和WS_2垂直异质结的生长为例, 拉曼光谱面扫图表明, ReS_2与WS_2是100%堆垛的(图4(k)和(l)); 理论计算也表明, ReS_2的生长只能在WS_2的(001)面进行, 两者表现出伴生生长的特殊行为. 通过这种方法生长出的异质结不存在界面污染以及氧化物残留的问题. 此外, 该方法还可实现其他TMDCs垂直异质结(MoS_2/WS_2异质结)的可控生长, 有望推动各种二维异质结及超晶格结构的生长及理论研究.

2.5 其他二维材料异质结

除了以上所述的异质结外, 石墨烯和TMDCs还可以与钙钛矿材料或稀土硫化物等组成异质结. Chen课题组[87]在CVD法制备的石墨烯上沉积EuS得到石墨烯/EuS异质结, 这种异质结改变了EuS磁绝缘的性质, 可以产生很大的交流磁场. Wu课题组[88]在CVD法制备的WS_2上用连续气相沉积法生长$CH_3NH_3PbI_3$, 得到$WS_2/CH_3NH_3PbI_3$异质结, 有效提升了光响应速度.

此外, 还有一些由新型二维材料构筑的异质结. 例如, 采用聚合物辅助的层层转移法构筑h-BN/BP/h-BN的三明治异质结, 一方面保护了BP, 另一方面又在磁场中表现出量子振荡行为[89]; 采用MBE制备得到的$HfTe_3/HfTe_5/Hf$异质结是一种包含超导体、拓扑绝缘体和普通金属的异质结, 可以表现出量子自旋霍尔(QSH)效应和拓扑相转变的性质[90].

3 二维材料异质结的应用

基于对可控制备方法的探索, 研究者获得了性能多样的二维材料异质结, 构筑了不同的结构和功能的二维材料异质结器件, 实现了对载流子传输的

控制、传输信号的存储, 以及对光信号的高灵敏响应[91]. 以下将从电子器件、光电器件等方面来介绍二维材料异质结的应用.

3.1 电子器件

基于二维材料异质结的电子器件主要分为记忆器件和FETs. 二者均由源极、漏极、沟道材料、栅极、栅极绝缘层组成, 记忆器件由于其需要存储载流子信号, 包含了浮动栅极控制存储过程, 而FETs的栅极则只用于调控载流子迁移行为. 一般只有二维材料垂直异质结才适用于记忆器件, 两层材料分别作为器件中的沟道和浮动栅极; 而二维材料的垂直异质结和面内异质结均可用于FETs, 一般只作为器件的沟道材料. 下面将分别介绍基于二维材料异质结的记忆器件和FETs, 并对其工作原理和性能进行评述.

记忆器件是一种可以擦写的存储电信号的器件, 是逻辑电路、集成电路、存储器中重要的器件之一. 一般非易失性记忆器件中主要结构为沟道材料、绝缘层、浮动栅极和控制栅极, 绝缘层主要用于隔开沟道材料和浮动栅极, 浮动栅极是载流子通过的通道, 调控栅极可控制载流子的流向, 沟道材料和浮动栅极组成异质结. Kis课题组[92]将多层石墨烯(MLG)和MoS_2分别作为浮动栅极和沟道材料, 用HfO_2作为绝缘层将二者隔开, 基于MLG/MoS_2异质结的非易失性记忆器件表现出了优秀的性能, 其程序写入和擦除的电流比为10^4, 且在+18 V的控制栅压下, 通过阈值电压-时间曲线估计10年后还能保有首次充电的30%. 结构类似的还有Zhang课题组[93]利用剥离法得到的BP/h-BN/MoS_2异质结构筑的记忆器件. 其中基底Si作为控制栅极, MoS_2作为浮动栅极, 调控栅极可以控制BP的载流子传输, 基于BP/h-BN/MoS_2异质结的非易失性记忆器件最大可以具有60 V的电压迟滞, 拥有较大的、可调控的记忆窗口. 以上的记忆器件均使用浮动栅极, 为三终端器件, 可实现快速记忆[94]. 然而, 器件结构的局限性和电路的复杂性限制了器件的可变性、扩展性和器件集成密度[95,96], 最近, Lee课题组[97]构筑了基于石墨烯/h-BN/MoS_2异质结的双终端隧道随机存取记忆器件(TRAM), 并详细解释了其工作过程. 器件结构如图5(a)所示, MoS_2作为沟道材料, 石墨烯作为浮动栅极, 合适厚度的h-BN作为隧穿绝缘层, 电荷可以隧穿到浮动栅极并在漏电极和浮动栅极的大电势下存储在浮动栅极中, 但不能从浮动栅极隧穿至源电极, 从而达到了存储信号的目的. 图5(b)是该器件在“程序写入-关态读取-擦除-开态读取”一个完整存取过程中的各处能带结构示意图、电荷传输示意图和器件各处电势分布情况. 程序写入过程, 当漏极加上–6 V电压时, 电子从漏极隧穿通过h-BN到达石墨烯并在石墨烯中进行传输, 但不能通过h-BN隧穿回源极, 整体电势为负; 关态读取过程时, 漏极电压为+0.1 V, 石墨烯的电势会比前一过程略低, 其中的捕获电子不会流出; 擦除时, 漏极电压为+6 V, 空穴会隧穿至浮动栅极中, 且不会隧穿回源极, 整体电势为正; 开态读取时, 漏极电压也为+0.1 V, 石墨烯电势比前一过程略高, 其中的捕获空穴不会流出. 此器件利用石墨烯作为浮动栅极, 在降低沟道长度的情况下, 将三终端简化为二终端记忆器件, 并且表现出10^{-14} A的超低关态电流和10^9的超高写入/擦除电流比, 经历10^5次以上循环也依然能保持较好性能, 实现了超高性能、超高稳定性的记忆器件构筑.

二维材料异质结除了在记忆器件方面表现出优异性能外, 在FETs方面也表现出了独特的性质. Kim课题组[63]构筑了基于WSe_2/MoS_2异质结双极性FET. 如图5(c)所示, FET的沟道部分为WSe_2/MoS_2异质结, 而其与源极和漏极的接触是不同的, WSe_2与Pt侧接触而MoS_2与Ti侧接触, 由于WSe_2和MoS_2分别为p型半导体和n型半导体, 所以WSe_2-Pt可以传输空穴, MoS_2-Ti可以传输电子. 图5(d)表示了单一MoS_2的FET、双极性FET在源漏电压分别为1和3 V的源漏电流和栅压的曲线, 说明双极性FET可在负栅压区域对载流子迁移的调控, 补充了单一MoS_2的FET在此区域无法调控载流子迁移的空白. 曲线中分为WSe_2传导区、耗散区、MoS_2传导区3个部分, 其传导机制如图5(e)所示, 当栅压为负时, 只有空穴进行传输, 显示为WSe_2传导, 而栅压为正时, 只有电子进行传输, 显示为MoS_2传导. 这种双极性FET通过控制栅压来控制载流子传输的类型, 弥补了单一TMDCs材料FET只能进行单一电子传输或空穴传输的不足.

Johnson课题组[62]在面内石墨烯/h-BN异质结上构筑了同源极多漏极的FET. 图6(a)显示了不同源漏电极的电导随栅压的变化曲线, 可以将曲线划分为2个区域, 这两个区域的曲线与图6(b)和(c)所示的不同源漏电极和对应沟道区域是一致的. 这表明石墨

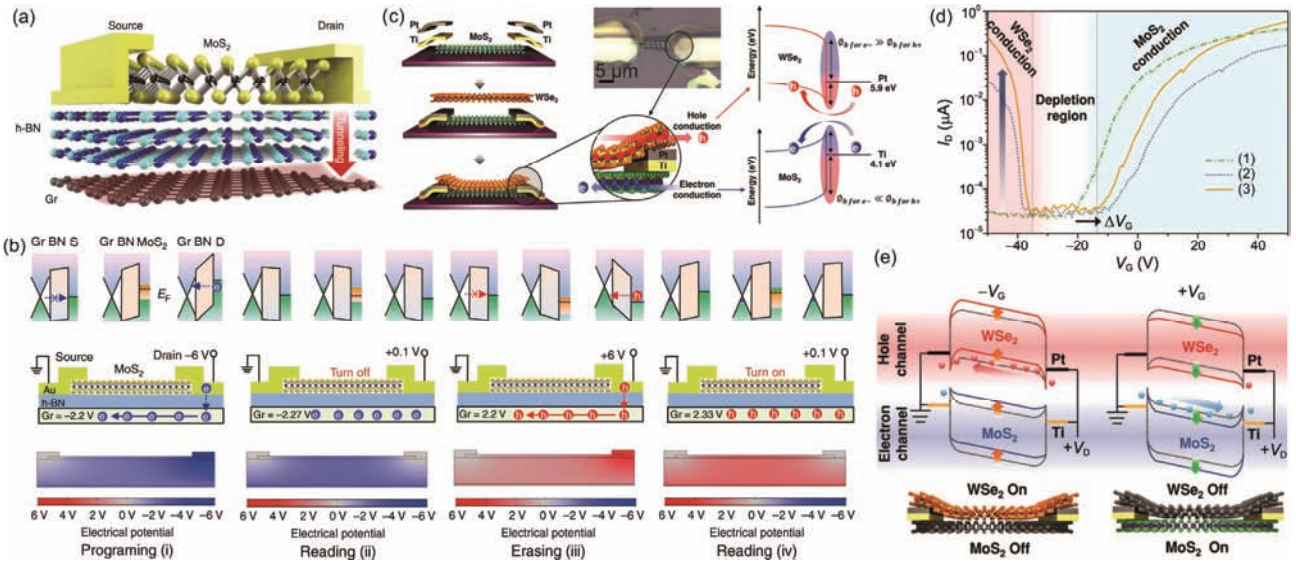

图 5 (网络版彩色)基于二维材料异质结的记忆器件和FET的示意图及工作机理. (a) 双终端TRAM器件示意图, 其中最上方的MoS_2作为沟道, 中间的h-BN作为隧穿绝缘层, 单层石墨烯作为浮动栅极. 箭头表示漏电极和石墨烯之间的电荷隧穿; (b) 双终端TRAM器件的能带示意图和电势分布的数值模拟[97]; (c) WSe_2/MoS_2异质结双沟道FET的构筑方法示意图和能带示意图; (d) 单沟道MoS_2的FET漏电流(I_D)-栅压(V_G)曲线 (曲线(1), 其漏电压(V_D)=1 V)和双沟道WSe_2/MoS_2异质结FET的I_D-V_G曲线(曲线(2), V_D=1 V; 曲线(3), V_D=3 V); (e) 双沟道WSe_2/MoS_2异质结FET在栅压为正和为负时的能带示意图[63]

Figure 5 (Color online) Schematic illustrations and working mechanism of 2D heterostructure-based memory cells and FETs. (a) Schematic of the two-terminal TRAM, in which MoS_2, h-BN and monolayer graphene are served as channel material, tunneling layer and floating gate, respectively. The arrow indicates the charge tunneling between drain electrode and graphene; (b) schematic band diagrams and numerical simulations of potential distribution in TRAM[97]; (c) schematic of fabrication process and band diagrams of the dual-channel FET based on WSe_2/MoS_2 heterostructure; (d) I_D-V_G curves of single-channel MoS_2 FET (curve (1), V_D=1 V) and dual-channel WSe_2/MoS_2 FET (curve (2), V_D=1 V; curve (3), V_D=3 V); (e) band diagrams of the dual-channel WSe_2/MoS_2 FET at positive and negative V_G[63]

烯/h-BN面内异质结与纯石墨烯之间的差异性主要体现在导电性和载流子迁移率等方面. 而基于石墨烯和h-BN的层层堆叠的垂直异质结, 隧穿场效应晶体管(TFET)也被成功构筑, 可用于高速石墨烯基模拟电子器件中[98].

Hone课题组[99]在透明柔性基底上构筑了基于MoS_2/石墨烯/h-BN异质结的柔性FET. 如图6(d)所示, 石墨烯作为栅极, h-BN作为绝缘层. 图6(e)表明, h-BN使得器件的导电性得到提高, 并使器件的迟滞得到降低; 当使用石墨烯作为栅极时, 如图6(f)所示, 由于电荷陷阱的缺少使得迟滞效应完全消失. 这种器件结构有效消除了电荷陷阱, 进而避免了迟滞效应的出现.

基于二维材料异质结的FET具有许多不同的结构, 可以发挥异质结不同的特性. 例如, 将多层WSe_2置于漏电极与石墨烯间形成的异质结, 可表现出5×10^7的超高开关电流比[100]; 采用离子凝胶作为栅极, 将MoS_2/石墨烯异质结的FET与WSe_2/石墨烯异质结的FET连接成的器件, 可以在窄至3 V的电压范围表现出高达3000 A cm^{-2}的电流密度和大于10^4的开关电流比[101]; 对于WSe_2进行热氧化形成WSe_2/WO_{3-x}面内异质结, 其迁移率相对于WSe_2有数十倍的提高[102]. 二维材料异质结还可以用于二极管中, 表现出独特的整流特性[103,104].

3.2 光电器件

大多数具有合适带隙的二维材料, 如大部分TMDCs和BP, 对光有比较明显的响应; 而石墨烯的高迁移率和高透光性、h-BN的洁净表面和低电荷陷阱均可以有效提高TMDCs和BP光响应性能. 因此, 二维材料异质结可以用于构筑光电检测器、光电二极管等器件, 并表现出光响应高、灵敏度高的优良性能.

Ye课题组[105]构筑了基于BP/MoS_2异质结的p-n二极管, 如图7(a)所示, 并将其用于光电检测中. 光电流随光照功率上升而上升, 并且最高可以表现出3×10^3的光/暗电流比. 此器件展现出良好的光响应性, 在正向和反向的偏压下, 分别表现出1.27 A W^{-1}和11 mA W^{-1}的响应率, 而在特定波长光照下最大可

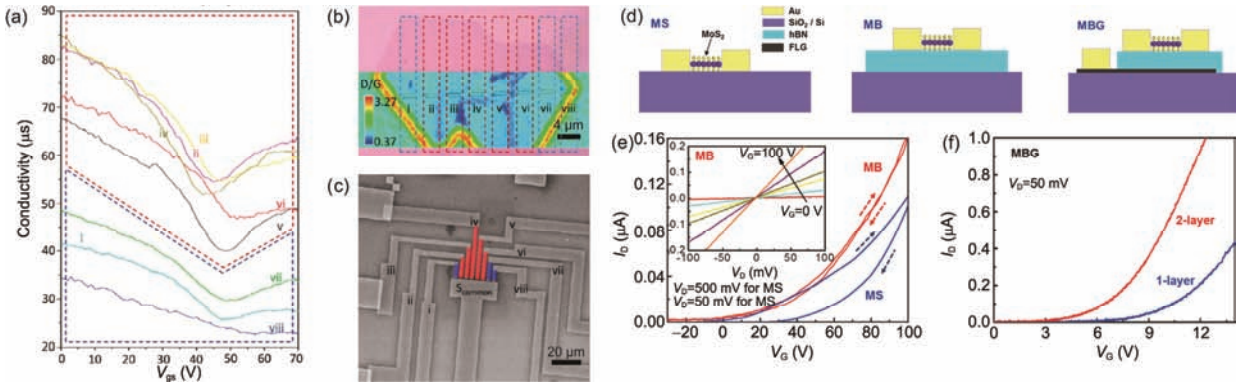

图 6 (网络版彩色)基于二维材料异质结的FETs的结构和性质. (a) 石墨烯/h-BN面内异质结FET的不同源漏电极区域的电导率随栅极电压的变化; (b) 异质结的光学显微图和拉曼光谱中D峰与G峰比值的拉曼面扫图; (c) 器件的SEM图, 器件有多个漏电极, 共用一个源电极[62]; (d) MoS_2, MoS_2/h-BN和MoS_2/h-BN/石墨烯FET的示意图; (e) MoS_2, MoS_2/h-BN的FET的I_D-V_G曲线, 插图是MoS_2/h-BN的FET的在不同栅压下的I_D-V_D曲线; (f) MoS_2/h-BN/石墨烯FET的迁移曲线, 厚层的MoS_2迁移率较高[99]

Figure 6 (Color online) Constructions and properties of 2D heterostructure-based FETs. (a) Conductivity-V_G curves of different area in a lateral graphene/h-BN heterostructure-based FET; (b) OM image and Raman mapping of D and G peak intensity ratio of the heterostructure; (c) SEM image of the FET with different drain electrodes and the same source electrode[62]; (d) schematic illustrations of MoS_2 FET, MoS_2/h-BN FET and MoS_2/h-BN/graphene FET; (e) I_D-V_G curves of MoS_2 FET and MoS_2/h-BN FET, and the inset shows I_D-V_D curves of MoS_2/h-BN FET at different V_G values; (f) transfer curves of MoS_2/h-BN/graphene FETs with MoS_2 of different thickness, in which the FET with a thicker MoS_2 shows a higher mobility[99]

以分别表现出3.54 A W^{-1}和418 mA W^{-1}的响应率, 是BP的100倍, 这说明MoS_2与BP构成的p-n异质结具有优异的光检测性能. 类似地, Xu课题组[106]利用基于BP/MoS_2的p-n异质结的光电检测器, 研究了器件各向异性的光响应性能. 他们采用波长分别为532和1550 nm的线性偏振激光进行照射, 发现两种波长激光均产生了各向异性的光电流强度, 但由于532 nm激光激发的是MoS_2的电子, 而1550 nm激光激发的是BP的电子, 所以二者的各向异性存在明显差异. 这说明, BP/MoS_2异质结也具有各向异性, 可以对不同方向入射光的产生不同的响应.

大多数基于二维材料异质结的FETs也具有良好的光电检测性能. Kim课题组[107]对构筑的石墨烯/MoS_2异质结FETs的沟道材料施加光照, 获得了不同波长入射光产生的源漏电流和栅压曲线, 其对520 nm波长光的最高响应率高达2.06×10^3 A W^{-1}, 表现出优异的光检测性能. Ferrari课题组[108]同样利用单层石墨烯和单层MoS_2组成异质结, 采用柔性基底和聚合物电解质, 构筑了柔性、高性能的光电检测器件, 如图7(b)和(c)所示. 图7(d)表示了器件中电子传输的机制, 当栅压为零时, 聚合物电解质两侧不带电, p型掺杂的单层石墨烯不涉及电子注入; 当栅压为负时, 聚合物电解质接触p型掺杂石墨烯的界面带负电, 石墨烯p型掺杂更高, 石墨烯/MoS_2界面电场增强, 会使MoS_2中电子转移至石墨烯中; 当栅压为正时, 聚合物电解质接触p型掺杂石墨烯的界面带正电, 石墨烯p型掺杂程度降低直至变为n型掺杂, 石墨烯/MoS_2界面电场减弱, 只有MoS_2中才能注入电子. 为了增加n型掺杂石墨烯沟道中的自由载流子浓度, 需要控制外部响应率和光电流的增量. 此光电检测器在栅压为−1~0.5 V时受光照电流降低, 在栅压大于0.5 V时, 石墨烯为n型掺杂, 受光照电流会略有升高, 并且在较弱光照、负栅压下可以观测到最大的外部响应率为5.5 A W^{-1}. 此器件最高可以达到45.5 A W^{-1}的外部响应率和570 A W^{-1}的内部响应率. 此外, 将此柔性光电检测器进行弯曲, 其光电流在不同弯曲程度和不同弯曲次数后变化不大(图7(e)~(g)). 这种光电检测器具有高响应性、柔性透明、低工作电压的优势, 因此有望应用于可穿戴、低能耗的光电器件中, 符合未来各类器件趋向于可穿戴化、智能化的要求.

由于钙钛矿材料具有良好的光响应性, 所以逐渐增加了钙钛矿材料与二维材料组成异质结构筑光电检测器的应用. 基于WS_2/$CH_3NH_3PbI_3$异质结的光电检测器中, WS_2传输电子, 而$CH_3NH_3PbI_3$传输空穴. 在无光照条件下, Au电极与二者的接触势垒很高, 电子难以从电极传输到WS_2中; 而在光照条件下, 光照使接触势垒降低, 从而使空穴和电子分别在两种材料中得以传输. 器件的响应率为17 A W^{-1}, 开关比可达3×10^5, 且器件的开关态响应速度快, 光电流从关到开和从开到关的弛豫时间仅2.7和7.5 ms[88]. 类似

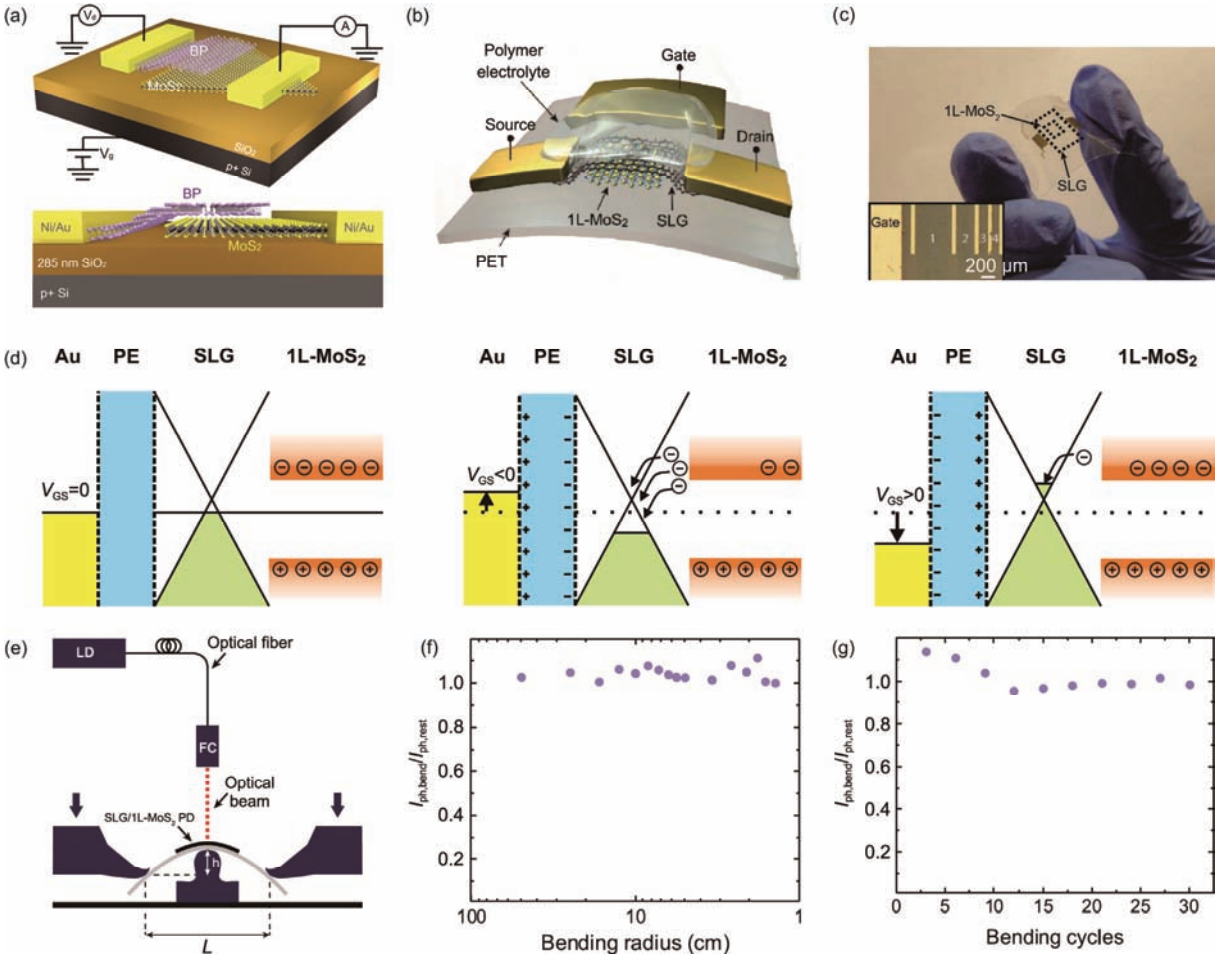

图 7 (网络版彩色)基于二维材料异质结的光电器件的结构示意图及工作机理. (a) BP/MoS_2异质结p-n二极管示意图[105]; (b) MoS_2/石墨烯异质结柔性光电检测器的示意图; (c) MoS_2/石墨烯异质结柔性光电检测器的照片; (d) MoS_2/石墨烯异质结柔性光电检测器在不同栅压时能带示意图; (e) 弯曲柔性测试的示意图; (f) 弯曲和未弯曲时的光电流比($I_{ph,bend}/I_{ph,rest}$)随弯曲半径的变化曲线; (g) $I_{ph,bend}/I_{ph,res}$随弯曲循环次数的变化曲线[108]

Figure 7 (Color online) Constructions and working mechanism of optoelectronics based on 2D heterostructures. (a) Schematic of the p-n diode based on BP/MoS_2 heterostructure[105]; (b) schematic illustration of the flexible photo detector based on MoS_2/graphene heterostructure; (c) the photo of the flexible photo detector based on MoS_2/graphene heterostructure; (d) band diagrams of the photo detector at different V_G values; (e) schematic three-point bending setup; (f) the $I_{ph,bend}/I_{ph,rest}$ towards different bending radius; (g) the change of $I_{ph,bend}/I_{ph,rest}$ towards bending cycles[108]

地，将单层WSe_2激光退火后组成$WSe_2/CH_3NH_3PbI_3$异质结可以表现出远高于本征单层$WSe_2/CH_3NH_3PbI_3$异质结、纯$CH_3NH_3PbI_3$和纯WSe_2光电检测器的响应率，高达1.1×10^5 mA W^{-1}[109]. 这为TMDCs/钙钛矿材料异质结用于光电检测器提供了一定的理论和实验基础，也展示了这种异质结在光电器件领域优秀的发展潜力.

3.3 其他应用

除了上述的电子器件和光电器件，二维材料异质结由于表面丰富的活性位点或特殊的电磁传导行为等还可用于传感器、拓扑绝缘体或光热器件等领域. Hahm课题组[110]利用石墨烯和MoS_2构筑异质结并实现了其在化学传感中的应用. 器件的示意图和SEM图如图8(a)和(b)所示. MoS_2与石墨烯电极组成异质结，其中MoS_2具有较多活性位点，可以吸附气体分子，而石墨烯导电性良好，可以较快传输电信号. 此传感器对于NO_2和NH_3均有良好的响应，分别能检测到浓度为1.2×10^{-6}的NO_2和5×10^{-6}的NH_3 (图8(c)和(d)). 将基底换成聚合物基底，还可以构筑柔性的气体传感器，为可穿戴的传感器奠定基础.

基于新型的二维超导体和拓扑绝缘体材料的异

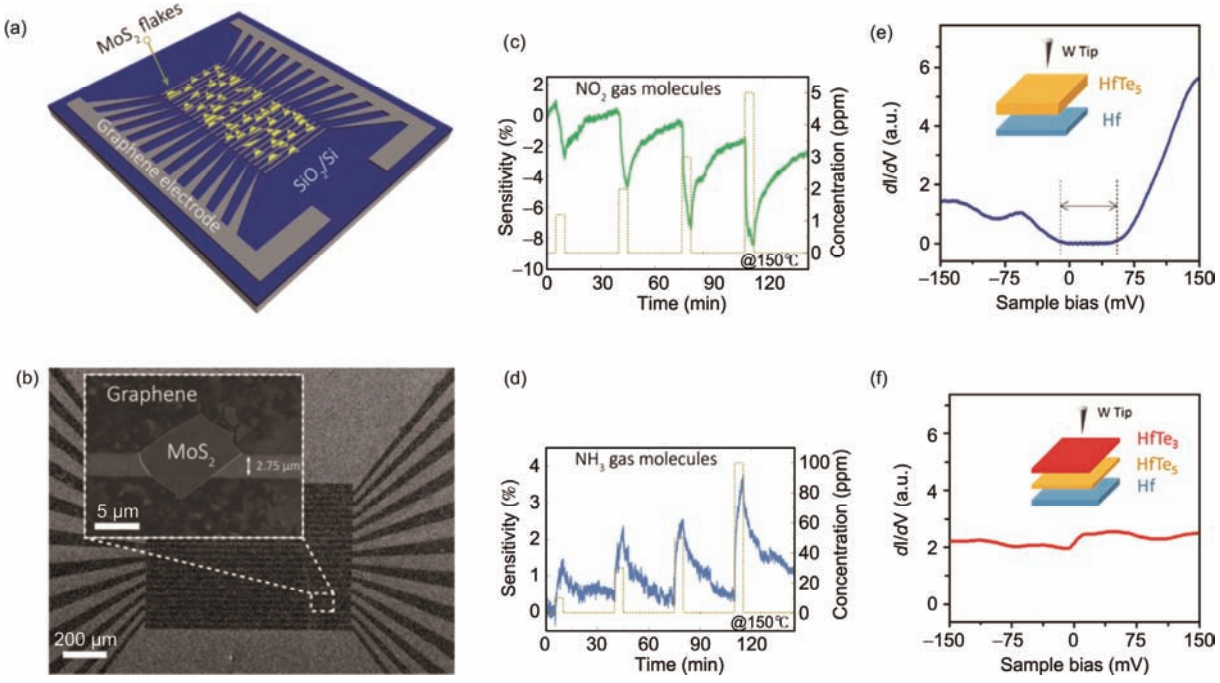

图 8 (网络版彩色)基于二维材料异质结的传感器及其他电学器件的结构与性质. (a) 图案化石墨烯电极上MoS_2的示意图; (b) 石墨烯电极集成的MoS_2器件的SEM图; 150℃时器件对NO_2(c)和NH_3(d)的瞬态响应[110]; 分别为$HfTe_5$/Hf异质结(e)和$HfTe_3$/$HfTe_5$/Hf异质结(f)的dI/dV与偏压的关系[90]

Figure 8 (Color online) Constructions and properties of sensors and other electronics based on 2D heterostructures. (a) Schematic of MoS_2 on patterned graphene electrodes; (b) SEM image of the MoS_2 device with integrated graphene electrodes; transient response to NO_2 (c) and NH_3 (d) at 150°C[110]; the differential tunneling conductance (dI/dV)-voltage bias curves of $HfTe_5$/Hf (e) and $HfTe_3$/$HfTe_5$/Hf (f) heterostructures[90]

质结可以构筑成具有特殊电导调控行为的器件. 例如, $HfTe_3$/$HfTe_5$/Hf异质结是超导体/拓扑绝缘体/金属异质结, 当$HfTe_5$/Hf组成异质结时, 微分隧穿电导(dI/dV)受到偏压调控(图8(e)), 而加入$HfTe_3$组成异质结后, dI/dV几乎不变(图8(f)). 这种异质结在QSH效应和拓扑相转变的研究中具有较大潜力[90].

二维材料异质结由于界面相互作用, 具有特殊的磁致电阻效应. 对于石墨烯/WS_2异质结, 其磁致电阻随磁场强度增大而增大, 同时也与载流子类型和密度有关(图9(a)); 如果异质结界面中存在粗糙起伏, 调控载流子类型会导致器件的磁致电阻-磁场强度曲线不重合, 这种现象可用于研究界面处相互作用[111]. 部分二维材料异质结所具有的磁致电阻效应还可应用于磁传感器领域. Yang课题组[112]构筑了石墨烯/h-BN异质结器件(图9(b)), 并发现其具有很明显的磁场响应的性质. 他们研究了磁场对器件的电阻-栅压曲线的影响, 当磁场强度为9 T时, 器件的电阻在栅压0~10 V附近出现一个峰值(图9(c)), 这说明器件的导电性与磁场强度关系密切. 在近电中性区, 施加9 T磁场时, 磁致电阻可以高达880%(图9(d)). 在不同栅压下, 霍尔电阻率随磁场变化也不同, 当栅压为正时, 霍尔电阻率随磁场变化斜率为负, 说明载流子主要为电子; 反之当栅压为负时, 载流子为空穴(图9(e)). 结果表明, 磁致电阻和霍尔电阻率可以反映载流子种类、浓度、迁移率的问题, 也说明某些具有高磁致电阻的二维材料异质结可以应用于磁场传感器或检测器中.

二维材料异质结还可以用于太赫兹纳米检测器[113]和等离子体调制[114]中. 总而言之, 二维材料异质结的应用涵盖了电学、光学、力学、热学等多个领域及其交叉领域, 在未来的生产生活中必然能占据一席之地.

4 机遇和挑战

二维材料异质结由于其独特、多样的性质被广泛关注, 目前已被证实可应用于电子、光电、传感等诸多领域. 然而采用主流的多次转移法难以获得高质量、大面积的二维材料异质结, 传统的CVD法制备的

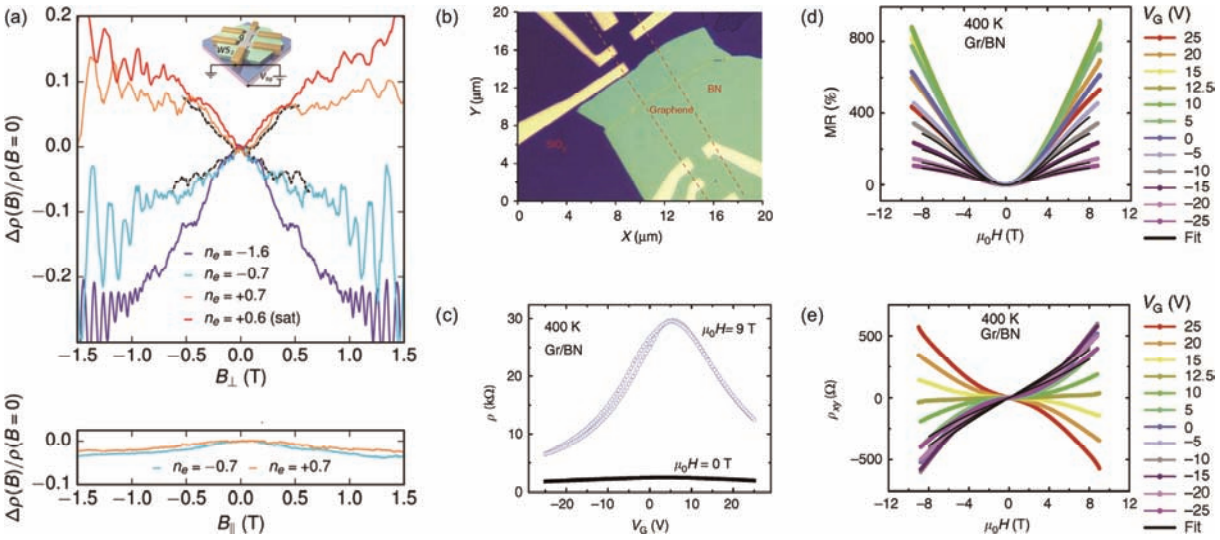

图 9 (网络版彩色)二维材料异质结的电磁器件结构与性质. (a) 石墨烯/WS_2异质结的磁致电阻对不同强度垂直磁场或平行磁场, 在不同载流子类型和密度的关系曲线[111]; (b) SiO_2上石墨烯/h-BN异质结器件光学显微图; (c) 石墨烯/h-BN异质结在0和9 T磁场时的电阻随栅压的变化曲线; (d), (e) 石墨烯/h-BN异质结在不同栅压下的磁致电阻和霍尔电阻率随磁场强度的变化曲线[112]

Figure 9 (Color online) Constructions and properties of 2D heterostructure-based electromagnetic devices. (a) Magnetoresistances of graphene/WS_2 heterostructure in different magnetic field for different carrier types and densities[111]; (b) OM image of a four-electrode device of graphene/h-BN heterostructure on SiO_2; (c) resistance-V_G curves of graphene/h-BN heterostructure at magnetic fields of 0 and 9 T, respectively; (d), (e) magnetoresistances and Hall resistivities towards different magnetic field of graphene/h-BN heterostructure at different V_G values[112]

二维材料异质结也存在界面污染等问题. 目前可控性较好、杂质残留较少的是共偏析法、LMCVD方法, 这些方法最大优势在于无界面污染且操作简便, 有望实现高质量二维材料异质结的大量制备. 此外, 二维材料异质结的应用受到目前器件加工技术的限制, 如电子束光刻、紫外光刻等技术引入的多种聚合物特别容易残留在二维材料异质结表面, 会严重影响器件的性能. 异质结阵列的制备和器件加工技术的发展与改进是二维材料异质结投入实际应用(如集成电路)必须面对的重大挑战.

参考文献

1 Novoselov K S, Geim A K, Morozov S V, et al. Electric field effect in atomically thin carbon films. Science, 2004, 306: 666–669
2 Morozov S V, Novoselov K S, Katsnelson M I, et al. Giant intrinsic carrier mobilities in graphene and its bilayer. Phys Rev Lett, 2008, 100: 016602
3 Banszerus L, Schmitz M, Engels S, et al. Ultrahigh-mobility graphene devices from chemical vapor deposition on reusable copper. Sci Adv, 2015, 1: e1500222
4 Xu M S, Liang T, Shi M M, et al. Graphene-like two-dimensional materials. Chem Rev, 2013, 113: 3766–3798
5 Xu H, Chen Y B, Zhang J, et al. Investigating the mechanism of hysteresis effect in graphene electrical field device fabricated on SiO_2 substrates using Raman spectroscopy. Small, 2012, 8: 2833–2840
6 Tan L F, Han J L, Mendes R G, et al. Self-aligned single-crystalline hexagonal boron nitride arrays: Toward higher integrated electronic devices. Adv Electron Mater, 2015, 1: 1500223
7 Novoselov K S, Mishchenko A, Carvalho A, et al. 2D materials and van der Waals heterostructures. Science, 2016, 353: aac9439
8 Xu H, Wu J X, Chen Y B, et al. Substrate engineering by hexagonal boron nitride/SiO_2 for hysteresis-free graphene FETs and large-scale graphene p-n junctions. Chem Asian J, 2013, 8: 2446–2452
9 Bolotin K I, Sikes K J, Jiang Z, et al. Ultrahigh electron mobility in suspended graphene. Solid State Commun, 2008, 146: 351–355
10 Lee C G, Wei X D, Kysar J W, et al. Measurement of the elastic properties and intrinsic strength of monolayer graphene. Science, 2008, 321: 385–388
11 Balandin A A, Ghosh S, Bao W Z, et al. Superior thermal conductivity of single-layer graphene. Nano Lett, 2008, 8: 902–907

12 Nair R R, Blake P, Grigorenko A N, et al. Fine structure constant defines visual transparency of graphene. Science, 2008, 320: 1308
13 Lu X K, Huang H, Nemchuk N, et al. Patterning of highly oriented pyrolytic graphite by oxygen plasma etching. Appl Phys Lett, 1999, 75: 193
14 Hernandez Y, Nicolosi V, Lotya M, et al. High-yield production of graphene by liquid-phase exfoliation of graphite. Nat Nanotechnol, 2008, 3: 563–568
15 Lu X K, Yu M F, Huang H, et al. Tailoring graphite with the goal of achieving single sheets. Nanotechnology, 1999, 10: 269–272
16 Zhou M, Wang Y L, Zhai Y M, et al. Controlled synthesis of large-area and patterned electrochemically reduced graphene oxide films. Chem Eur J, 2009, 15: 6116–6120
17 Gao W, Alemany L B, Ci L J, et al. New insights into the structure and reduction of graphite oxide. Nat Chem, 2009, 1: 403–408
18 Huang H, Chen W, Chen S, et al. Bottom-up growth of epitaxial graphene on 6H-SiC(0001). ACS Nano, 2008, 2: 2513–2518
19 Emtsev K V, Bostwick A, Horn K, et al. Towards wafer-size graphene layers by atmospheric pressure graphitization of silicon carbide. Nat Mater, 2009, 8: 203–207
20 Zhang Q, Tan L F, Chen Y X, et al. Human-like sensing and reflexes of graphene-based films. Adv Sci, 2016, 3: 1600130
21 Zeng M Q, Wang L X, Liu J X, et al. Self-assembly of graphene single crystals with uniform size and orientation: The first 2D super-ordered structure. J Am Chem Soc, 2016, 138: 7812–7815
22 May J W. Platinum surface LEED rings. Surf Sci, 1969, 17: 267–270
23 Geim A K. Graphene: Status and prospects. Science, 2009, 324: 1530–1534
24 Allen M J, Tung V C, Kaner R B. Honeycomb carbon: A review of graphene. Chem Rev, 2010, 110: 132–145
25 Kim J Y, Kim F K, Huang J X. Seeing graphene-based sheets. Mater Today, 2010, 13: 28–38
26 Chhowalla M, Shin H S, Eda G, et al. The chemistry of two-dimensional layered transition metal dichalcogenide nanosheets. Nat Chem, 2013, 5: 263–275
27 Wang Q H, Kalantar-Zadeh K, Kis A, et al. Electronics and optoelectronics of two-dimensional transition metal dichalcogenides. Nat Nanotechnol, 2012, 7: 699–712
28 Cao T, Wang G, Han W P, et al. Valley-selective circular dichroism of monolayer molybdenum disulphide. Nat Commun, 2012, 3: 887
29 Zeng H L, Dai J F, Yao W, et al. Valley polarization in MoS_2 monolayers by optical pumping. Nat Nanotechnol, 2012, 7: 490–493
30 Splendiani A, Sun L, Zhang Y B, et al. Emerging photoluminescence in monolayer MoS_2. Nano Lett, 2010, 10: 1271–1275
31 Mak K F, Lee C G, Hone J, et al. Atomically thin MoS_2: A new direct-gap semiconductor. Phys Rev Lett, 2010, 105: 136805
32 Golberg D, Bando Y, Huang Y, et al. Boron nitride nanotubes and nanosheets. ACS Nano, 2010, 4: 2979–2993
33 Dean C R, Young A F, Meric I, et al. Boron nitride substrates for high-quality graphene electronics. Nat Nanotechnol, 2010, 5: 722–726
34 Watanabe K, Taniguchi T, Kanda H. Direct-bandgap properties and evidence for ultraviolet lasing of hexagonal boron nitride single crystal. Nat Mater, 2004, 3: 404–409
35 Kim K K, Hsu A, Jia X T, et al. Synthesis and characterization of hexagonal boron nitride film as a dielectric layer for graphene devices. ACS Nano, 2012, 6: 8583–8590
36 Zhang C H, Fu L, Zhao S L, et al. Controllable co-segregation synthesis of wafer-scale hexagonal boron nitride thin films. Adv Mater, 2014, 26: 1776–1781
37 Gao Y, Ren W C, Ma T, et al. Repeated and controlled growth of monolayer, bilayer and few-layer hexagonal boron nitride on Pt foils. ACS Nano, 2013, 7: 5199–5206
38 Salvatore G A, Munzenrieder N, Barraud C, et al. Fabrication and transfer of flexible few-layers MoS_2 thin film transistors to any arbitrary substrate. ACS Nano, 2013, 7: 8809–8815
39 Li X M, Yin J, Zhou J X, et al. Large area hexagonal boron nitride monolayer as efficient atomically thick insulating coating against friction and oxidation. Nanotechnology, 2014, 25: 105701
40 Liu Z, Gong Y J, Zhou W, et al. Ultrathin high-temperature oxidation-resistant coatings of hexagonal boron nitride. Nat Commun, 2013, 4: 2541
41 Husain E, Narayanan T N, Taha-Tijerina J J, et al. Marine corrosion protective coatings of hexagonal boron nitride thin films on stainless steel. ACS Appl Mater Interfaces, 2013, 5: 4129–4135
42 Watanabe K, Taniguchi T, Niiyama T, et al. Far-ultraviolet plane-emission handheld device based on hexagonal boron nitride. Nat Photon, 2009, 3: 591–594
43 Kubota Y, Watanabe K, Tsuda O, et al. Deep ultraviolet light-emitting hexagonal boron nitride synthesized at atmospheric pressure. Science, 2007, 317: 932–934
44 Lebègue S, Eriksson O. Electronic structure of two-dimensional crystals fromab initiotheory. Phys Rev B, 2009, 79: 115409
45 De Padova P, Quaresima C, Ottaviani C, et al. Evidence of graphene-like electronic signature in silicene nanoribbons. Appl Phys Lett, 2010, 96: 261905

46 Lalmi B, Oughaddou H, Enriquez H, et al. Epitaxial growth of a silicene sheet. Appl Phys Lett, 2010, 97: 223109

47 Persichetti L, Jardali F, Vach H, et al. Van der Waals heteroepitaxy of germanene islands on graphite. J Phys Chem Lett, 2016, 7: 3246–3251

48 Derivaz M, Dentel D, Stephan R, et al. Continuous germanene layer on Al(111). Nano Lett, 2015, 15: 2510–2516

49 Zhu F F, Chen W J, Xu Y, et al. Epitaxial growth of two-dimensional stanene. Nat Mater, 2015, 14: 1020–1025

50 Tao L, Cinquanta E, Chiappe D, et al. Silicene field-effect transistors operating at room temperature. Nat Nanotechnol, 2015, 10: 227–231

51 Bayani A H, Dideban D, Vali M, et al. Germanene nanoribbon tunneling field effect transistor (GeNR-TFET) with a 10 nm channel length: Analog performance, doping and temperature effects. Semicond Sci Technol, 2016, 31: 045009

52 Zhu J J, Chroneos A, Schwingenschlogl U. Silicene/germanene on MgX_2 (X=Cl, Br, and I) for Li-ion battery applications. Nanoscale, 2016, 8: 7272–7277

53 Liu H, Neal A T, Zhu Z, et al. Phosphorene: An unexplored 2D semiconductor with a high hole mobility. ACS Nano, 2014, 8: 4033–4041

54 Woomer A H, Farnsworth T W, Hu J, et al. Phosphorene: Synthesis, scale-up, and quantitative optical spectroscopy. ACS Nano, 2015, 9: 8869–8884

55 Morita A. Semiconducting black phosphorus. Appl Phys A Solids Surfaces, 1986, 39: 227–242

56 Wood J D, Wells S A, Jariwala D, et al. Effective passivation of exfoliated black phosphorus transistors against ambient degradation. Nano Lett, 2014, 14: 6964–6970

57 Tai G A, Hu T S, Zhou Y G, et al. Synthesis of atomically thin boron films on copper foils. Angew Chem Int Ed, 2015, 54: 15473–15477

58 Halim J, Kota S, Lukatskaya M R, et al. Synthesis and characterization of 2D molybdenum carbide (MXene). Adv Funct Mater, 2016, 26: 3118–3127

59 Xu C, Wang L B, Liu Z B, et al. Large-area high-quality 2D ultrathin Mo_2C superconducting crystals. Nat Mater, 2015, 14: 1135–1141

60 Li X F, Basile L, Huang B, et al. Van der Waals epitaxial growth of two-dimensional single-crystalline GaSe domains on graphene. ACS Nano, 2015, 9: 8078–8088

61 Wang Y, Wang S S, Lu Y H, et al. Strain-induced isostructural and magnetic phase transitions in monolayer MoN_2. Nano Lett, 2016, 16: 4576–4582

62 Han G H, Rodriguez-Manzo J A, Lee C W, et al. Continuous growth of hexagonal graphene and boron nitride in-plane heterostructures by atmospheric pressure chemical vapor deposition. ACS Nano, 2013, 7: 10129–10138

63 Lee I Y, Rathi S, Lim D S, et al. Gate-tunable hole and electron carrier transport in atomically thin dual-channel WSe_2/MoS_2 heterostructure for ambipolar field-effect transistors. Adv Mater, 2016, 28: 9519–9525

64 Barton A T, Yue R, Anwar S, et al. Transition metal dichalcogenide and hexagonal boron nitride heterostructures grown by molecular beam epitaxy. Microelectron Eng, 2015, 147: 306–309

65 Chen K, Wan X, Xie W G, et al. Lateral built-in potential of monolayer MoS_2-WS_2 in-plane heterostructures by a shortcut growth strategy. Adv Mater, 2015, 27: 6431–6437

66 Yan A M, Velasco J J, Kahn S, et al. Direct growth of single- and few-layer MoS_2 on h-BN with preferred relative rotation angles. Nano Lett, 2015, 15: 6324–6331

67 Fu L, Sun Y Y, Wu N, et al. Direct growth of MoS_2/h-BN heterostructures via a sulfide-resistant alloy. ACS Nano, 2016, 10: 2063–2070

68 Zhang T, Jiang B, Xu Z, et al. Twinned growth behavior of two-dimensional materials. Nat Commun, 2016, 7: 13911

69 Xu Z G, Zheng R J, Khanaki A, et al. Direct growth of graphene on *in situ* epitaxial hexagonal boron nitride flakes by plasma-assisted molecular beam epitaxy. Appl Phys Lett, 2015, 107: 213103

70 Zhang C H, Zhao S L, Jin C H, et al. Direct growth of large-area graphene and boron nitride heterostructures by a co-segregation method. Nat Commun, 2015, 6: 6519

71 Liu Z, Tizei L H, Sato Y, et al. Postsynthesis of h-BN/graphene heterostructures inside a STEM. Small, 2016, 12: 252–259

72 Wu Q K, Jang S K, Park S, et al. *In situ* synthesis of a large area boron nitride/graphene monolayer/boron nitride film by chemical vapor deposition. Nanoscale, 2015, 7: 7574–7579

73 Wang S S, Wang X C, Warner J H. All chemical vapor deposition growth of MoS_2:h-BN vertical van der Waals heterostructures. ACS Nano, 2015, 9: 5246–5254

74 Behura S, Nguyen P, Che S W, et al. Large-Area, transfer-free, oxide-assisted synthesis of hexagonal boron nitride films and their heterostructures with MoS_2 and WS_2. J Am Chem Soc, 2015, 137: 13060–13065

75 Cattelan M, Markman B, Lucchini G, et al. New strategy for the growth of complex heterostructures based on different 2D materials. Chem Mater, 2015, 27: 4105–4113

76 Zhang M, Zhu Y M, Wang X S, et al. Controlled synthesis of ZrS_2 monolayer and few layers on hexagonal boron nitride. J Am Chem Soc, 2015, 137: 7051–7054

77 Shi Y M, Zhou W, Lu A Y, et al. Van der Waals epitaxy of MoS_2 layers using graphene as growth templates. Nano Lett, 2012, 12: 2784–2791
78 Miwa J A, Dendzik M, Gronborg S S, et al. Van der Waals epitaxy of two-dimensional MoS_2-graphene heterostructures in ultrahigh vacuum. ACS Nano, 2015, 9: 6502–6510
79 Liu X L, Balla I, Bergeron H, et al. Rotationally commensurate growth of MoS_2 on epitaxial graphene. ACS Nano, 2016, 10: 1067–1075
80 Lin Y C, Lu N, Perea-Lopez N, et al. Direct synthesis of van der Waals solids. ACS Nano, 2014, 8: 3715–3723
81 Ago H, Fukamachi S, Endo H, et al. Visualization of grain structure and boundaries of polycrystalline graphene and two-dimensional materials by epitaxial growth of transition metal dichalcogenides. ACS Nano, 2016, 10: 3233–3240
82 Shi J P, Liu M X, Wen J X, et al. All chemical vapor deposition synthesis and intrinsic bandgap observation of MoS_2/graphene heterostructures. Adv Mater, 2015, 27: 7086–7092
83 Li M Y, Shi Y M, Cheng C C, et al. Epitaxial growth of a monolayer WSe_2-MoS_2 lateral p-n junction with an atomically sharp interface. Science, 2015, 349: 524–528
84 Gong Y J, Lin J H, Wang X L, et al. Vertical and in-plane heterostructures from WS_2/MoS_2 monolayers. Nat Mater, 2014, 13: 1135–1142
85 Yoo Y D, Degregorio Z P, Johns J E. Seed crystal homogeneity controls lateral and vertical heteroepitaxy of monolayer MoS_2 and WS_2. J Am Chem Soc, 2015, 137: 14281–14287
86 Gong Y J, Lei S D, Ye G L, et al. Two-step growth of two-dimensional WSe_2/$MoSe_2$ heterostructures. Nano Lett, 2015, 15: 6135–6141
87 Wei P, Lee S W, Lemaitre F, et al. Strong interfacial exchange field in the graphene/EuS heterostructure. Nat Mater, 2016, 15: 711–716
88 Ma C, Shi Y M, Hu W J, et al. Heterostructured WS_2/$CH_3NH_3PbI_3$ photoconductors with suppressed dark current and enhanced photodetectivity. Adv Mater, 2016, 28: 3683–3689
89 Chen X L, Wu Y Y, Wu Z F, et al. High-quality sandwiched black phosphorus heterostructure and its quantum oscillations. Nat Commun, 2015, 6: 7315
90 Wang Y Q, Wu X, Wang Y L, et al. Spontaneous formation of a superconductor-topological insulator-normal metal layered heterostructure. Adv Mater, 2016, 28: 5013–5017
91 Liu Y, Weiss N O, Duan X D, et al. Van der Waals heterostructures and devices. Nat Rev Mater, 2016, 1: 16042
92 Bertolazzi S, Krasnozhon D, Kis A. Nonvolatile memory cells based on MoS_2/graphene heterostructures. ACS Nano, 2013, 7: 3246–3252
93 Li D, Wang X J, Zhang Q C, et al. Nonvolatile floating-gate memories based on stacked black phosphorus-boron nitride-MoS_2 heterostructures. Adv Funct Mater, 2015, 25: 7360–7365
94 Kahng D, Sze S M. A floating gate and its application to memory devices. Bell Sys Technol J, 1967, 46: 1288–1295
95 Zhao C, Zhao C Z, Taylor S, et al. Review on non-volatile memory with high-k dielectrics: Flash for generation beyond 32 nm. Materials, 2014, 7: 5117–5145
96 Sekitani T, Yokota T, Zschieschang U, et al. Organic nonvolatile memory transistors for flexible sensor arrays. Science, 2009, 326: 1516–1519
97 Vu Q A, Shin Y S, Kim Y R, et al. Two-terminal floating-gate memory with van der Waals heterostructures for ultrahigh on/off ratio. Nat Commun, 2016, 7: 12725
98 Britnell L, Gorbachev R V, Jalil R, et al. Field-effect tunneling transistor based on vertical graphene heterostructures. Science, 2012, 335: 947–950
99 Lee G H, Yu Y J, Cui X, et al. Flexible and transparent MoS_2 field-effect transistors on hexagonal boron nitride-graphene heterostructures. ACS Nano, 2013, 7: 7931–7936
100 Shim J W, Kim H S, Shim Y S, et al. Extremely large gate modulation in vertical graphene/WSe_2 heterojunction barristor based on a novel transport mechanism. Adv Mater, 2016, 28: 5293–5299
101 Choi Y S, Kang J M, Jariwala D, et al. Low-voltage complementary electronics from ion-gel-gated vertical van der Waals heterostructures. Adv Mater, 2016, 28: 3742–3748
102 Liu B L, Ma Y Q, Zhang A Y, et al. High-performance WSe_2 field-effect transistors via controlled formation of in-plane heterojunctions. ACS Nano, 2016, 10: 5153–5160
103 Kim W J, Li C F, Chaves F A, et al. Tunable graphene-GaSe dual heterojunction device. Adv Mater, 2016, 28: 1845–1852
104 Jeon P J, Lee Y T, Lim J Y, et al. Black phosphorus-zinc oxide nanomaterial heterojunction for p-n diode and junction field-effect transistor. Nano Lett, 2016, 16: 1293–1298
105 Deng Y X, Luo Z, Conrad N J, et al. Black phosphorus-monolayer MoS_2 van der Waals heterojunction p-n diode. ACS Nano, 2014, 8: 8292–8299
106 Hong T, Chamlagain B, Wang T J, et al. Anisotropic photocurrent response at black phosphorus-MoS_2 p-n heterojunctions. Nanoscale, 2015, 7: 18537–18541

107 Rathi S, Lee I Y, Lim D S, et al. Tunable electrical and optical characteristics in monolayer graphene and few-layer MoS_2 heterostructure devices. Nano Lett, 2015, 15: 5017–5024

108 De Fazio D, Goykhman I, Yoon D H, et al. High responsivity, large-area graphene/MoS_2 flexible photodetectors. ACS Nano, 2016, 10: 8252–8262

109 Lu J P, Carvalho A, Liu H W, et al. Hybrid bilayer WSe_2-$CH_3NH_3PbI_3$ organolead halide perovskite as a high-performance photodetector. Angew Chem Int Ed, 2016, 55: 11945–11949

110 Cho B J, Yoon J W, Lim S K, et al. Chemical sensing of 2D graphene/MoS_2 heterostructure device. ACS Appl Mater Interfaces, 2015, 7: 16775–16780

111 O'Farrell E C, Avsar A, Tan J Y, et al. Quantum transport detected by strong proximity interaction at a graphene-WS_2 van der Waals interface. Nano Lett, 2015, 15: 5682–5688

112 Gopinadhan K, Shin Y J, Jalil R, et al. Extremely large magnetoresistance in few-layer graphene/boron-nitride heterostructures. Nat Commun, 2015, 6: 8337

113 Viti L, Hu J, Coquillat D, et al. Heterostructured hBN-BP-hBN nanodetectors at terahertz frequencies. Adv Mater, 2016, 28: 7390–7396

114 Zhang K, Yap F L, Li K, et al. Large scale graphene/hexagonal boron nitride heterostructure for tunable plasmonics. Adv Funct Mater, 2014, 24: 731–738

Summary for “二维材料异质结的可控制备及应用”

Controllable synthesis of two dimensional heterostructures and their application

XIAO Yao[1], JIANG Bei[2], YANG KeNa[2], ZHANG Tao[2] & FU Lei[1,2*]

[1] *The Institute for Advanced Studies, Wuhan University, Wuhan 430072, China;*
[2] *College of Chemistry and Molecular Science, Wuhan University, Wuhan 430072, China*
* Corresponding author, E-mail: leifu@whu.edu.cn

Since the successful exfoliation of graphene in 2004, many attentions have been paid to two-dimensional (2D) materials, which include graphene, h-BN, transition metal dichalcogenides (TMDCs), black phosphorus (BP) and so on. Although these materials have shown unique characteristics, there are numerous challenges in this emerging field. For example, charge trap between the substrate and the 2D materials seriously influences their excellent electrical properties; some 2D materials are unstable while exposed in air, which will lead to their degradation. To have an intensive study of the basic properties of 2D materials and broaden their field of application, researchers pay attentions to the heterostructures of these materials, which consist of vertically stacked or laterally pieced 2D materials, including graphene/h-BN, TMDCs/h-BN, TMDCs/graphene, and TMDCs/TMDCs heterostructures, et al. For vertical heterostructures, graphene/h-BN vertical heterostructures mainly take advantage of h-BN to decrease the charge trap between insulating layer and graphene, thus to increase the carrier mobility in graphene. TMDCs/graphene vertical heterostructures mainly combine the good photo responsivity of TMDCs with the high conductivity of graphene, which can be utilized for high performance optoelectronics. TMDCs/TMDCs vertical heterostructures mainly combine the band structures of two different materials to control the carrier transport behavior, thus realizing excellent carrier storage or high performance photo responsivity. Lateral heterostructures are only suitable for materials with low lattice mismatch, and they are usually used for studying the carrier transport behavior between the interfaces of materials. Along with the increasing requirements on integration and multifunction, 2D heterostructures-based electronic and optoelectronic devices are paid much more attention to. Controllable synthesis of 2D heterostructures is the precondition of constructions of high-performance and highly-integrated devices. This review first introduces the preparation methods of 2D materials, including exfoliation, molecular beam epitaxy (MBE) and chemical vapor deposition (CVD). Exfoliation method mainly pieces the exfoliated materials together to form heterostructures with the help of polymer. MBE can overcome the difficulties of the transfer process in exfoliation, however they are not suitable for large scale preparation. Compared with exfoliation and MBE, CVD has less restrictions on the substrate, as well as a simple preparation process with lower cost and higher quality of the as-prepared materials. 2D heterostructures can be prepared by the combination of exfoliation and CVD, or CVD process only. Then, considering the problem of the interface contamination in these preparation methods proposed at present, we put forward a liquid metal strategy in the controllable preparation of 2D heterostructures. Furthermore, we introduce the construction and performance of 2D-heterostructures-based electronic and optical devices. The opportunities and challenges in the preparation and application of 2D heterostructures are also discussed.

two dimensional heterostructures, exfoliation, chemical vapor deposition, electronics, optoelectronics

doi: 10.1360/N972016-01348